

Interactions between Rydberg excitons in Cu₂O

Valentin Walther,¹ Sjard Ole Krüger,² Stefan Scheel,² and Thomas Pohl¹

¹*Department of Physics and Astronomy, Aarhus University,
Ny Munkegade 120, DK 8000 Aarhus C, Denmark*

²*Institut für Physik, Universität Rostock, Albert-Einstein-Straße 23, D-18059 Rostock, Germany*

Highly-excited states of excitons in cuprous oxide have recently been observed at a record quantum number of up to $n = 25$. Here, we evaluate the long-range interactions between pairs of Rydberg excitons in Cu₂O, which are due to direct Coulomb forces rather than short-range collisions typically considered for ground state excitons. A full numerical analysis is supplemented by the van der Waals asymptotics at large exciton separations, including the angular dependence of the potential surfaces.

I. INTRODUCTION

Excitons play an important role for the optical properties of many semiconductors. Composed of an electron and a hole bound by their Coulomb attraction, excitons may be considered as artificial atoms that feature a series of energy levels very similar to that of simple one-electron atoms. Their relatively low exciton binding energies combined with additional effects such as phonon coupling¹ or crystal inhomogeneities, however, render the observation of excited exciton states inherently difficult. Cuprous oxide (Cu₂O) stands out in this respect, as it features a comparably large Rydberg energy of ~ 86 meV, which together with the narrow absorption lines provides well-suited conditions for exciting excitonic Rydberg states. In fact, recent measurements on Cu₂O semiconductors² have demonstrated the preparation of highly-excited Rydberg excitons with record-breaking principal quantum numbers of up to $n = 25$. This discovery has sparked renewed theoretical and experimental interest in the field of excitons, ranging from excitonic spectra in magnetic³ and electric^{4,5} fields as well as non-atomic scaling laws⁶ to the breaking of all antiunitary symmetries⁷ and the onset of quantum chaos⁸.

A further particular appeal of such Rydberg states stems from their strong mutual interactions, which, as demonstrated for cold atomic systems⁹, can lead to enhanced optical nonlinearities of the material¹⁰. In contrast to ground-state excitons whose low-energy interactions can often be described in terms of zero-range collisions^{11,12}, the interaction between Rydberg excitons can become important already on much larger length scales and lead to an exciton blockade² that prevents the optical excitation of two excitons within typical distances of several μm . Under such conditions the relevant interactions are no longer dominated by exchange effects¹¹ but are determined by direct Coulomb interactions between the excitons.

In this work, we determine the interaction between Rydberg excitons in Cu₂O. Our calculations account for the dipole-dipole coupling between energetically close exciton pair states that is induced by their direct Coulomb interaction and dominates the overall interaction at the large distances relevant under experimental conditions² of Rydberg exciton blockade. Asymptotically, the interaction

is of van der Waals type with a van der Waals coefficient that is found to follow a simple scaling law which was previously used for Rydberg state interactions of alkaline¹³ and alkaline earth atoms¹⁴. From our calculations, we determine the corresponding scaling coefficients, providing easy access to precise values of Rydberg-exciton van der Waals coefficients in Cu₂O for future studies of many-body effects or nonlinear optical phenomena due to interactions between highly-excited excitons.

The article is organized as follows. After outlining the determination of Rydberg exciton wave functions from the semiconductor band structure in Sec. (II), we describe our calculations of the direct Coulomb pair interaction in Sec. (III). The obtained potential energy curves are discussed in Sec. (IV), where we present the perturbative calculation of the van der Waals interactions and summarize our results for the van Waals coefficients for a broad range different excitonic Rydberg states. Finally, implications, limitations and potential applications of the results are discussed in Sec. (V).

II. SINGLE EXCITON STATES

Bulk Cu₂O is a semiconductor with a cubic crystal structure of the point group O_h and a direct band gap of $E_g = 2.17208$ eV at the center of its Brillouin zone². Without spin, the uppermost valence band has Γ_5^+ symmetry, which is split into an upper Γ_7^+ - and a lower Γ_8^+ -band by the spin-orbit interaction. These two bands are separated by a corresponding spin-orbit splitting of $\Delta = 131$ meV and can be described by an effective band Hamiltonian derived in Ref.¹⁵.

Together with the lowest Γ_6^+ conduction band, these valence bands form two excitonic series: the so-called yellow ($\Gamma_6^+ \otimes \Gamma_7^+$) and green ($\Gamma_6^+ \otimes \Gamma_8^+$) series. The optical transition from the excitonic vacuum to the s -excitons is dipole forbidden for both series due to the positive parity of both the conduction and the valence band. The series of interest to this work is the yellow series whose p -exciton resonances are located below the band gap and have been observed experimentally².

We determine the exciton binding energies, $E_{\mathbf{K},nl}$, and wave functions, $\tilde{\Psi}(\mathbf{K},\mathbf{k})$, from the nonparabolic

momentum-space Wannier equation

$$\left[\frac{\hbar^2 (\alpha \mathbf{K} + \mathbf{k})^2}{2m_e} + T_h (|\beta \mathbf{K} - \mathbf{k}|^2) \right] \tilde{\Psi}(\mathbf{K}, \mathbf{k}) + \frac{e^2}{8\pi^3 \varepsilon_0 \varepsilon_r} \int d^3 \mathbf{k}' \frac{\tilde{\Psi}(\mathbf{K}, \mathbf{k}')}{|\mathbf{k} - \mathbf{k}'|^2} = E \tilde{\Psi}(\mathbf{K}, \mathbf{k}) \quad (1)$$

as described in Ref.¹⁶. Here, the hole's dispersion T_h is obtained from an angular average over the hole dispersion derived from the valence band Hamiltonian of Ref.¹⁵ and ε_0 denotes the vacuum permittivity, while $\varepsilon_r \approx 7.5$ is the static relative permittivity of Cu_2O . Furthermore, \mathbf{k} and \mathbf{K} denote the relative and center-of-mass (COM) momentum of the electron-hole pair, respectively, and $\alpha = m_e/M$ and $\beta = m_h/M$ denote the mass of the electron (m_e) and the hole (m_h) in units of the total exciton mass $M = m_e + m_h$.

The nonparabolicity of the hole dispersion T_h plays an important role for the bound state properties and yields the leading contribution to the excitonic quantum defect¹⁶. Its effect on the center-of-mass dynamics with momentum K can, however, be neglected as long as $K \ll \pi/a_l$, where a_l is the lattice constant. This approximation is well justified because the momentum of the optical photon that generates the exciton is much smaller than π/a_l . Therefore, we can separate the relative and COM part of the exciton wave function, whose real-space representation can consequently be written as

$$\Psi_{\mathbf{K},nlm}(\mathbf{R}, \mathbf{r}) = \frac{1}{\sqrt{V}} e^{i\mathbf{K}\cdot\mathbf{R}} \psi_{nlm}(\mathbf{r}), \quad (2)$$

with corresponding energies

$$E_{\mathbf{K},nl} = \frac{\hbar^2 \mathbf{K}^2}{2M} + E_{0,nl}. \quad (3)$$

Moreover, $\mathbf{R} = \alpha \mathbf{r}_e + \beta \mathbf{r}_h$ and $\mathbf{r} = \mathbf{r}_e - \mathbf{r}_h$, as illustrated Fig. 1a, and $\psi_{nlm}(\mathbf{r})$ denotes the bound-state wave function obtained from the extended Wannier equation with the standard quantum numbers n , l and m .

As we have assumed rotational symmetry and neglected the non-parabolic COM dispersion, the excitonic states are degenerate with regard to the magnetic quantum number m . The anisotropy of the valence band can be included in this calculation and would lead to further splitting of states with $l \geq 2$. The size of this splitting depends on the momentum-space extension and scales roughly with n^{-3} . The same is true for exchange-splitting of the S-excitons and both effects are neglected in this work, as they are of minor importance to the Rydberg states of interest.

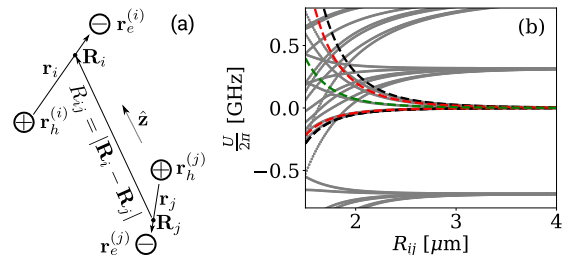


FIG. 1. a) Sketch of a pair of excitons i and j , consisting of electrons at $\mathbf{r}_e^{(i,j)}$ and holes at $\mathbf{r}_h^{(i,j)}$. The center of mass coordinates are indicated by $\mathbf{R}_{i,j}$, the exciton separation by R_{ij} . The coordinate system is aligned with $\hat{\mathbf{z}}$. b) Potential energy surfaces centered around $n = 15p$ with corresponding van-der-Waals curves. The thin lines are obtained from a numerical diagonalization, whereas the colored lines show the asymptotic results for the different families of M with $|M| = 0$ (black), $|M| = 1$ (red), $|M| = 2$ (green).

III. RYDBERG EXCITON INTERACTION POTENTIAL

The pairwise interaction between excitons is given by the sum

$$V^{(ij)} = \frac{e^2}{4\pi\varepsilon_0\varepsilon_r} \left(\frac{1}{|\mathbf{r}_e^{(i)} - \mathbf{r}_e^{(j)}|} + \frac{1}{|\mathbf{r}_h^{(i)} - \mathbf{r}_h^{(j)}|} - \frac{1}{|\mathbf{r}_e^{(i)} - \mathbf{r}_h^{(j)}|} - \frac{1}{|\mathbf{r}_e^{(j)} - \mathbf{r}_h^{(i)}|} \right) \quad (4)$$

of mutual Coulomb interactions between the electron and hole of one exciton at respective positions $\mathbf{r}_e^{(i)}$ and $\mathbf{r}_h^{(i)}$, respectively, and another electron-hole pair at positions $\mathbf{r}_e^{(j)}$ and $\mathbf{r}_h^{(j)}$. Within a multipole expansion, the interaction can be rewritten¹³ as a series of inverse powers of the exciton COM distance $R_{ij} = |\mathbf{R}_i - \mathbf{R}_j|$

$$V^{(ij)} = \frac{e^2}{4\pi\varepsilon_0\varepsilon_r} \sum_{l,L=1}^{\infty} \frac{\mathcal{V}_{lL}(\mathbf{r}_i, \mathbf{r}_j)}{R_{ij}^{l+L+1}}, \quad (5)$$

where

$$\mathcal{V}_{lL}(\mathbf{r}_i, \mathbf{r}_j) = \frac{(-1)^L 4\pi}{\sqrt{(2l+1)(2L+1)}} r_i^l r_j^L \sum_m \sqrt{\binom{l+L}{l+m} \binom{l+L}{L+m}} Y_{lm}(\hat{\mathbf{r}}_i) Y_{L-m}(\hat{\mathbf{r}}_j) \quad (6)$$

and Y_{lm} denotes the spherical harmonics defined with respect to the distance vector \mathbf{R}_{ij} .

While the interaction between ground-state excitons¹¹ can be often estimated from first-order perturbation theory, by evaluating Coulomb scattering matrix elements based on Hartree-Fock states for pairs of interacting excitons, such an approximation¹⁷ becomes inapplicable for

excitonic Rydberg states whose large polarizability^{2,9,18} requires a non-perturbative treatment of the Coulomb interactions. In this regime, the exciton interaction predominantly stems from the virtual dipole-dipole coupling between exciton bound states while exchange effects are negligibly small. This is typically the case for exciton distances¹⁹

$$R_{ij} \gg 2 \cdot \left(\sqrt{\langle r_i^2 \rangle} + \sqrt{\langle r_j^2 \rangle} \right). \quad (8)$$

Note that this condition also ensures convergence of the above multipole expansion, Eq. (5), which for sufficiently large distances is predominantly determined by the dipole-dipole contribution $l = L = 1$, such that

$$V^{(ij)} \approx \frac{e^2}{4\pi\epsilon_0\epsilon_r} \left(\frac{r_i r_j}{R_{ij}^3} - \frac{3(\mathbf{r}_i \cdot \mathbf{R}_{ij})(\mathbf{r}_j \cdot \mathbf{R}_{ij})}{R_{ij}^5} \right) \quad (9)$$

We proceed by expanding the resulting Hamiltonian for the two interacting excitons in a pair product basis $|\mathbf{s}_i, \mathbf{s}_j\rangle = |n_i l_i m_i, n_j l_j m_j\rangle$ composed of the single-exciton states $\psi_{n_i, l_i, m_i}(\mathbf{r}_i)$ and $\psi_{n_j, l_j, m_j}(\mathbf{r}_j)$, discussed in Sec. II. The adiabatic Born-Oppenheimer potentials are then obtained by diagonalizing the resulting internal-state Hamiltonian for a given exciton distance R_{ij} . Its diagonal elements are given by $E_{0, n_i l_i} + E_{0, n_j l_j}$ while the off-diagonal coupling terms $\langle \mathbf{s}_i, \mathbf{s}_j | V^{(ij)} | \mathbf{s}'_i, \mathbf{s}'_j \rangle$ are calculated using Eq. (9). We choose a quantization that is aligned with \mathbf{R}_{ij} , such that the total angular momentum $M = m_i + m_j$ is conserved and remains a good quantum number for the two-exciton states in the presence of interaction.

The numerical diagonalization then yields potential energy surfaces $U_\mu(R_{ij})$ and associated two-exciton states $|\mu(R_{ij})\rangle$. Examples of the resulting interaction curves are shown in Fig. 1(b) for exciton-pair states around the $15p$ asymptote for different values of M . The relevant values of n , l and m are dictated by the band symmetry and the chosen excitation scheme as well as the frequency and polarization of the involved excitation lasers. The polarization of the laser that drives the Rydberg state transition defines another axis that generally can have a finite angle with the chosen quantization axis aligned along the distance vector \mathbf{R}_{ij} , such that the optical coupling strength can depend on the orientation of the exciton pair through the state composition of the two-exciton state $|\mu(R_{ij})\rangle$, as discussed below.

IV. EXCITONIC VAN DER WAALS INTERACTIONS

The interaction potential and associated two-exciton states assume a simple form for large distances R_{ij} where

$$\left| \langle \mathbf{s}_i, \mathbf{s}_j | V^{(ij)} | \mathbf{s}'_i, \mathbf{s}'_j \rangle \right| \ll \left| E_{0, n_i l_i} + E_{0, n_j l_j} - E_{0, n'_i l'_i} - E_{0, n'_j l'_j} \right| \quad (10)$$

such that the dipole-dipole interaction only induces a weak far off-resonant coupling to other exciton pair states. Due to the aforementioned interaction blockade of exciton excitation, this condition can be satisfied in previous Cu_2O experiments². We can thus apply degenerate second-order perturbation theory in the form of an effective operator

$$\begin{aligned} \hat{H}_{\text{vdW}} &= \left(\frac{e^2}{4\pi\epsilon_0\epsilon_r R_{ij}^3} \right)^2 \sum_{|\alpha\rangle \notin \mathcal{M}} \frac{\hat{V}_{11}^{(ij)} |\alpha\rangle \langle \alpha| \hat{V}_{11}^{(ij)}}{\delta} \\ &= \sum_{\mu} \frac{C_6^\mu}{R_{ij}^6} |\mu\rangle \langle \mu| \end{aligned} \quad (11)$$

whose action is restricted to the degenerate subspaces $\mathcal{M} = \{|\mathbf{s}_i, \mathbf{s}_j\rangle\}$ of fixed l and M at energy \bar{E}^{18} . Here $\delta = 2\bar{E} - E_\alpha$ is the Förster defect, while the two-exciton eigenstates $|\mu\rangle$ are now independent of the distance R_{ij} but can still be composed of several pair states $|\mathbf{s}_i, \mathbf{s}_j\rangle$. As shown in Fig. 1(b) for $n = 15$, the van der Waals interaction potential obtained in this way provides an excellent description of our numerical results already for $R \gtrsim 2.5 \mu\text{m}$.

Figure 2 and Tab. I summarize our results for the van der Waals interaction between Cu_2O Rydberg excitons with angular momenta $l = 0$ (s), $l = 1$ (p) and $l = 2$ (d). The simplest asymptote is that of two s -excitons. With only one asymptotic state $|n00, n00\rangle$, Eq. (11) reduces to standard non-degenerate perturbation theory. For higher angular momenta, $l > 0$, however, the degenerate pair states get mixed by the interaction as given in Tab. (I). The results are invariant with respect to the sign of M , reflecting the corresponding symmetry of the exciton pair.

This leaves a total of $2l + 1$ different $|M\rangle$ -states for a given l and $2l + 1 - |M|$ states within each of the $(l, |M|)$ -manifolds, which are indicated by different colors in Fig. 1(b). The depicted van der Waals coefficients and associated eigenstates have been obtained by diagonalizing Eq. (11) in each $(l, |M|)$ -subspace. While the result of this calculation may in general depend on the precise value of the principal quantum number n through the corresponding coupling strengths to other pair states and their relative energy separation, the obtained eigenstates turn out to be virtually independent of n (cf. standard deviations given in Tab. (I)).

The van der Waals interaction rapidly increases with the principal quantum number n . This is due to the quadratic increase of the dipole matrix elements for transitions between Rydberg states and the decreasing level spacing, such that $\delta \sim n^{-3}$, which overall results in an increase of the van der Waals coefficient as $C_6 \sim n^{11}$. Similar to the behavior of atomic systems¹³, our numerical results can be well described by the slightly modified scaling relation

$$C_6(n) = n^{11} (c_0 + c_1 n^1 + c_2 n^2), \quad (12)$$

whose coefficients c_i depend on the angular numbers and are given in Tab. I. As shown in Fig. 2, this simple ex-

[M]	composition of $ns - ns$ asymptote	$\frac{c_0}{2\pi}$ [mHz μm^6] $\times 10^1$	$\frac{c_1}{2\pi}$ [mHz μm^6] $\times 10^2$	$\frac{c_2}{2\pi}$ [mHz μm^6] $\times 10^3$
0	$ \frac{n00}{n00} \rangle$	-2.046	-0.672	0.125
[M]	composition of $np - np$ asymptote			
2	$ \frac{n11}{n11} \rangle$	1.257	3.641	-0.666
1	$\frac{1}{\sqrt{2}}(\frac{n10}{n11} \rangle - \frac{n11}{n10} \rangle)$	5.853	8.372	-1.503
1	$\frac{1}{\sqrt{2}}(\frac{n10}{n11} \rangle + \frac{n11}{n10} \rangle)$	-3.574	0.680	-0.160
0	$(-0.252 \pm 0.003)(\frac{n1-1}{n11} \rangle + \frac{n11}{n1-1} \rangle) +$ $(0.934 \pm 0.001) \frac{n10}{n10} \rangle$	8.159	11.549	-2.067
0	$\frac{1}{\sqrt{2}}(\frac{n1-1}{n11} \rangle - \frac{n11}{n1-1} \rangle)$	-3.456	-0.205	0.006
0	$(0.661 \pm 0.001)(\frac{n1-1}{n11} \rangle + \frac{n11}{n1-1} \rangle) +$ $(0.356 \pm 0.004) \frac{n10}{n10} \rangle$	-4.371	0.608	-0.143
[M]	composition of $nd - nd$ asymptote			
4	$ \frac{n22}{n22} \rangle$	6.247	4.067	-0.719
3	$\frac{1}{\sqrt{2}}(\frac{n21}{n22} \rangle + \frac{n22}{n21} \rangle)$	-2.201	-1.936	0.481
3	$\frac{1}{\sqrt{2}}(\frac{n21}{n22} \rangle - \frac{n22}{n21} \rangle)$	10.906	7.237	-1.317
2	$-0.429(\frac{n20}{n22} \rangle + \frac{n22}{n20} \rangle) + 0.795 \frac{n21}{n21} \rangle$	14.881	9.862	-1.807
2	$\frac{1}{\sqrt{2}}(\frac{n20}{n22} \rangle - \frac{n22}{n20} \rangle)$	1.536	0.650	-0.018
2	$0.562(\frac{n20}{n22} \rangle + \frac{n22}{n20} \rangle) + 0.607 \frac{n21}{n21} \rangle$	-4.005	-3.752	0.889
1	$0.218(\frac{n2-1}{n22} \rangle - \frac{n22}{n2-1} \rangle) - 0.673(\frac{n20}{n21} \rangle - \frac{n21}{n20} \rangle)$	17.480	11.564	-2.125
1	$(-0.465 \pm 0.001)(\frac{n2-1}{n22} \rangle + \frac{n22}{n2-1} \rangle) +$ $(0.533 \pm 0.001)(\frac{n20}{n21} \rangle + \frac{n21}{n20} \rangle)$	4.604	2.582	-0.373
1	$(0.533 \pm 0.001)(\frac{n2-1}{n22} \rangle + \frac{n22}{n2-1} \rangle) +$ $(0.465 \pm 0.001)(\frac{n20}{n21} \rangle + \frac{n21}{n20} \rangle)$	-3.559	-3.905	0.954
1	$-0.673(\frac{n2-1}{n22} \rangle - \frac{n22}{n2-1} \rangle) - 0.218(\frac{n20}{n21} \rangle - \frac{n21}{n20} \rangle)$	-2.017	-2.208	0.567
0	$-0.082(\frac{n2-2}{n22} \rangle + \frac{n22}{n2-2} \rangle) +$ $0.451(\frac{n2-1}{n21} \rangle + \frac{n21}{n2-1} \rangle) - 0.762 \frac{n20}{n20} \rangle$	18.386	12.153	-2.234
0	$(-0.222 \pm 0.001)(\frac{n2-2}{n22} \rangle - \frac{n22}{n2-2} \rangle) +$ $0.671(\frac{n2-1}{n21} \rangle - \frac{n21}{n2-1} \rangle)$	5.559	3.240	-0.501
0	$(0.343 \pm 0.004)(\frac{n2-2}{n22} \rangle + \frac{n22}{n2-2} \rangle) +$ $(-0.448 \pm 0.003)(\frac{n2-1}{n21} \rangle + \frac{n21}{n2-1} \rangle) +$ $(-0.603 \pm 0.001) \frac{n20}{n20} \rangle$	-0.146	-1.315	0.434
0	$(0.613 \pm 0.002)(\frac{n2-2}{n22} \rangle + \frac{n22}{n2-2} \rangle) +$ $(0.311 \pm 0.003)(\frac{n2-1}{n21} \rangle + \frac{n21}{n2-1} \rangle) +$ $(0.236 \pm 0.004) \frac{n20}{n20} \rangle$	-3.861	-4.031	0.956
0	$-0.671(\frac{n2-2}{n22} \rangle - \frac{n22}{n2-2} \rangle) +$ $(-0.222 \pm 0.001)(\frac{n2-1}{n21} \rangle - \frac{n21}{n2-1} \rangle)$	-3.736	-3.639	0.850

TABLE I. Various asymptotes listed by quantum numbers l, M with corresponding approximate asymptotic wavefunctions and van der Waals coefficients $C_6(n) = n^{11}(c_0 + c_1n + c_2n^2)$ as obtained from fitting for principal quantum numbers $n = 12-25$. The given errors are standard deviations calculated from the numerically obtained eigenfunctions.

pression permits an accurate determination of the van der Waals interaction for the depicted range $12 \lesssim n \lesssim 25$.

The van der Waals coefficients of the $np - np$ asymptotes for $n = 11$, however, show slightly larger deviations. This is due to the $np + np \rightarrow (n-1)d + (n+1)d$ coupling channel, which becomes near resonant around $n = 11$ as shown in Fig. 3(a). As the denominator in Eq. (11) goes through a minimum, the resulting van der Waals interaction is enhanced, while the validity of Eq. (11) requires

larger exciton distances. However, a comparison with our numerical results [Fig. 3(b)] shows that the agreement remains good even at relatively small exciton separations of $\sim 1\mu\text{m}$, comparable to what is also required for $n = 12$ in the absence of the Förster resonance.

An interesting and often relevant situation arises when an external field introduces an axis that is not parallel to the intermolecular axis \mathbf{R}_{ij} . Examples include electric and magnetic fields as well as a tilted excitation laser,

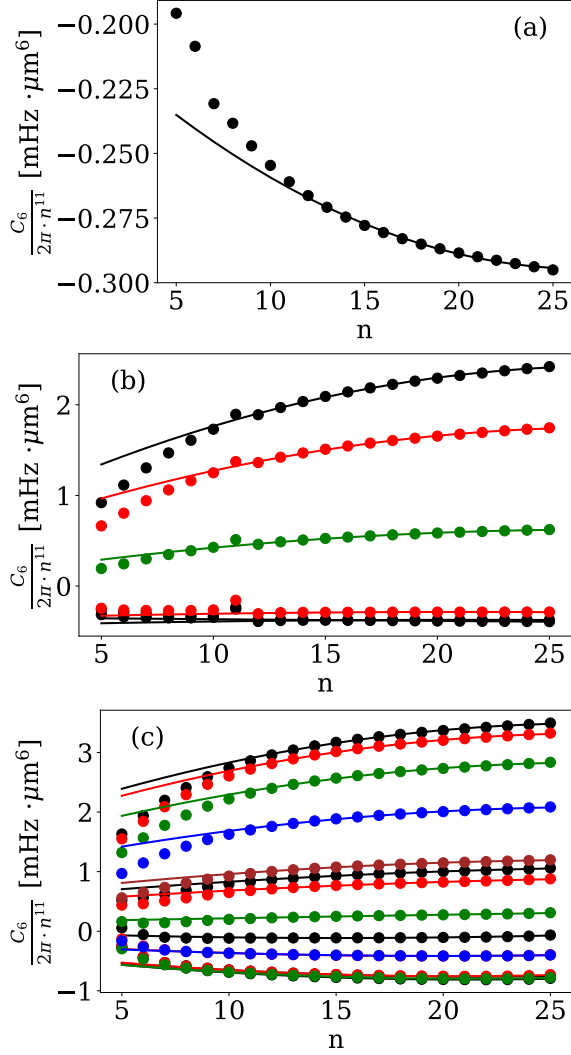


FIG. 2. C_6 values for a) the $s-s$, b) $p-p$ and c) $d-d$ asymptotes. The fits are for extrapolation for $n \geq 12$. Colored lines denote the families of M with $|M| = 0$ (black), $|M| = 1$ (red), $|M| = 2$ (green), $|M| = 3$ (blue), $|M| = 4$ (brown).

each defining a new axis \hat{z}^{lab} . Without loss of generality, we assume that the molecular axis lies in the (x, z) -plane of the laboratory frame, such that the two \hat{z} -axes span the interaction angle θ ²⁰. A general transformation of the states between the frames is given by

$$|nlm\rangle^{\text{mol}} = \sum_{m'} [d_{mm'}^l(\theta)]^* |nlm'\rangle^{\text{lab}}, \quad (13)$$

where $d_{mm'}^l(\theta)$ denotes elements of the lowercase Wigner d-matrix²¹. While it is often advantageous to express the external field in the molecular frame, we illustrate the angular dependence by evaluating the optical coupling strengths of the $p-p$ asymptotic pair states in the laboratory frame. For a definite laser polarization, only certain pair states are optically active and the optical

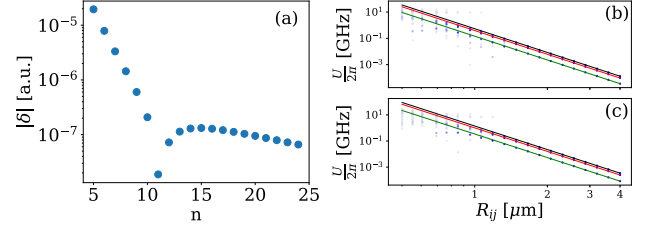


FIG. 3. At $n = 11$ a near Förster resonance in the channel $np + np \rightarrow (n-1)d + (n+1)d$ leads to outlying points in the otherwise quite homogeneous range of $C_6(n)$. b) The Förster defect δ of the given channel passes zero near $n = 11$. Taking the repulsive part of the interaction as an example, the numerical solution (blue dots) is compared with the long-range asymptote with $|M| = 0$ (black), $|M| = 1$ (red), $|M| = 2$ (green) for $n = 11$ (b) and $n = 12$ (c). The color code denotes the relative p -component of each asymptote. Despite of the near resonance at $n = 11$, their difference is small as long as $R \gtrsim 1\mu\text{m}$ since the dominant channels fall into the van der Waals regime.

coupling, given by the their overlap with the optically active pair state, becomes a function of θ (Fig. 4).

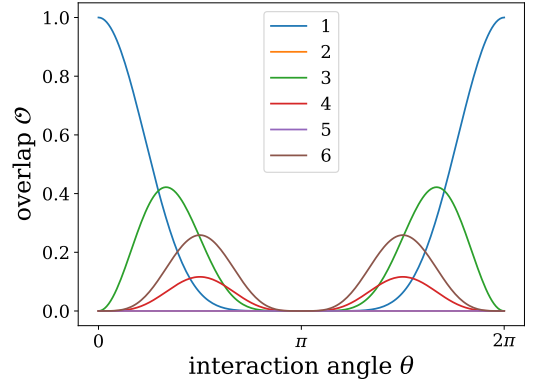


FIG. 4. Overlap of the optically active pair state ϕ_a with the asymptotic molecular eigenstates $|\mu\rangle$, $\mathcal{O} = |\langle\phi_a|\mu\rangle|^2$. Here, for illustration, we chose $|\phi_a\rangle = |n11, n11\rangle$ for σ^+ -light and the eigenstates of the $p-p$ -asymptote (labeled as listed in Tab. I). Note that antisymmetric states 2 and 5 do not couple to the excitation laser.

V. DISCUSSION

In summary, we have evaluated the interaction between Rydberg excitons in Cu_2O semiconductors and provided an expression that, together with the tabulated parameters, facilitates a simple and yet accurate determination of the resulting van der Waals interaction for a broad range of Rydberg states. Such van der Waals interactions may be responsible for the recently observed² excitation

blockade of excitons in Cu₂O. The highest lying exciton state reported in these experiments ($n = 25$) covers a 4 million times larger volume than the $2p$ -exciton state, owing to the $\sim n^2$ scaling of the exciton radius. Such a large radius entails an even higher enhancement of the polarizability as $\sim n^7$, such that electrostatic interactions become relevant at exciton separations where exchange effects are negligible.

The importance of long-range dipole interactions for Rydberg excitons is connected to the way they are created by optical excitation. Shifts of the Rydberg pair-state energy due to exciton-exciton interactions can inhibit the simultaneous generation of Rydberg excitons within a certain radius once they exceed the width of the corresponding exciton line. For strong interactions and sufficiently narrow excitation lines, this excitation blockade effect thus ensures that excitons are only created at distances where van der Waals interactions dominate. This may open up a new regime where strong interaction effects become observable at very low densities of excitons, which therefore interact over long distances in a quasi-static fashion, as opposed to short-range collisional interactions that determine the behaviour of ground-state excitons. The accurate knowledge of van der Waals interactions between Rydberg excitons, as provided by the present work, enables quantitative theoretical studies of this blockade effect. This in turn would also make it possible to estimate the importance of other mechanisms such as interactions with the free charges of potentially forming electron-hole plasmas⁴ and to thereby determine their relative contribution to the nonlinear optical response of the semiconductor.

One major difference between the typical scales of Rydberg states of excitons and atomic Rydberg states stems from the effective electron and hole masses as well as the dielectric constant, ϵ_r , of the semiconductor. Both factors tend to decrease the binding energy and lead to a decrease of the Rydberg constant by a factor $\nu = \mu_X/(\mu_A\epsilon_r^2)$, where μ_X and μ_A denote the reduced mass of the excitonic and atomic system, respectively. On the other hand, the excitonic radius is increased by a factor $(\epsilon_r\nu)^{-1}$. Therefore we expect the van der Waals coefficient to increase as $\sim \epsilon_r^4\mu_A^5/\mu_X^5$. Accordingly, the van der Waals coefficients as calculated in the present work exceed those of typical atomic Rydberg states with comparable quantum numbers^{13,14} by 5 orders of magnitude. This also opens the search for other suitable semiconductor systems with Rydberg states^{22,23}, each featuring different interaction properties and additional rich physics²⁴.

Rydberg excitons thus suggest promising avenues to studies of strong interaction effects in confined geometries²⁵, optical nonlinearities¹⁰ or nonclassical light generation^{26,27} at ultralow exciton densities. The results of the present work provide simple yet accurate interaction potentials for future theoretical explorations of these perspectives.

VI. ACKNOWLEDGEMENT

We would like to thank the authors of Ref.²⁰ for sharing their Rydberg potential software “pairinteraction”, parts of which we used in the exact diagonalization. We are grateful to the DFG SPP 1929 GiRyd for financial support.

-
- ¹ F. Schweiner, J. Main, and G. Wunner, Phys. Rev. B **93**, 085203 (2016).
- ² T. Kazimierzczuk, D. Fröhlich, S. Scheel, H. Stolz, and M. Bayer, Nature **514**, 343 (2014).
- ³ S. Zielińska-Raczyńska, D. Ziemkiewicz, and G. Czajkowski, Phys. Rev. B **95**, 075204 (2017).
- ⁴ J. Heckötter, M. Freitag, D. Fröhlich, M. Aßmann, M. Bayer, M. A. Semina, and M. M. Glazov, Phys. Rev. B **95**, 035210 (2017).
- ⁵ S. Zielińska-Raczyńska, D. Ziemkiewicz, and G. Czajkowski, Phys. Rev. B **94**, 045205 (2016).
- ⁶ J. Heckötter, M. Freitag, D. Fröhlich, M. Aßmann, M. Bayer, M. A. Semina, and M. M. Glazov, Phys. Rev. B **96**, 125142 (2017).
- ⁷ F. Schweiner, J. Main, and G. Wunner, Phys. Rev. Lett. **118**, 046401 (2017).
- ⁸ M. Aßmann, J. Thewes, D. Fröhlich, and M. Bayer, Nature Materials **15**, 741 EP (2016), article.
- ⁹ M. Saffman, T. G. Walker, and K. Mølmer, Rev. Mod. Phys. **82**, 2313 (2010).
- ¹⁰ V. Walther, R. Johne, and T. Pohl, Nature communications **9**, 1309 (2018).
- ¹¹ C. Ciuti, V. Savona, C. Piermarocchi, A. Quattropani, and P. Schwendimann, Phys. Rev. B **58**, 7926 (1998).
- ¹² F. Tassone and Y. Yamamoto, Phys. Rev. B **59**, 10830 (1999).
- ¹³ K. Singer, J. Stanojevic, M. Weidemüller, and R. Côté, Journal of Physics B: Atomic, Molecular and Optical Physics **38**, S295 (2005).
- ¹⁴ R. Mukherjee, J. Millen, R. Nath, M. P. A. Jones, and T. Pohl, Journal of Physics B: Atomic, Molecular and Optical Physics **44**, 184010 (2011).
- ¹⁵ K. Suzuki and J. C. Hensel, Phys. Rev. B **9**, 4184 (1974).
- ¹⁶ F. Schöne, S.-O. Krüger, P. Grünwald, H. Stolz, S. Scheel, M. Aßmann, J. Heckötter, J. Thewes, D. Fröhlich, and M. Bayer, Phys. Rev. B **93**, 075203 (2016).
- ¹⁷ V. Shahnazaryan, I. A. Shelykh, and O. Kyriienko, Phys. Rev. B **93**, 245302 (2016).
- ¹⁸ T. G. Walker and M. Saffman, Phys. Rev. A **77**, 032723 (2008).
- ¹⁹ R. J. L. Roy, Canadian Journal of Physics **52**, 246 (1974), <https://doi.org/10.1139/p74-035>.
- ²⁰ S. Weber, C. Tresp, H. Menke, A. Urvoy, O. Firstenberg, H. P. Büchler, and S. Hofferberth, Journal of Physics B: Atomic, Molecular and Optical Physics **50**, 133001 (2017).
- ²¹ E. Wigner, *Group theory and its application to the quantum mechanics of atomic spectra* (Academic Press, 1959).

- ²² A. Chernikov, T. C. Berkelbach, H. M. Hill, A. Rigosi, Y. Li, O. B. Aslan, D. R. Reichman, M. S. Hybertsen, and T. F. Heinz, *Physical review letters* **113**, 076802 (2014).
- ²³ P. T. Greenland, S. A. Lynch, A. F. G. van der Meer, B. N. Murdin, C. R. Pidgeon, B. Redlich, N. Q. Vinh, and G. Aeppli, *Nature* **465**, 1057 EP (2010).
- ²⁴ G. Wang, A. Chernikov, M. M. Glazov, T. F. Heinz, X. Marie, T. Amand, and B. Urbaszek, *Rev. Mod. Phys.* **90**, 021001 (2018).
- ²⁵ S. O. Krüger and S. Scheel, *Phys. Rev. B* **97**, 205208 (2018).
- ²⁶ G. Muñoz-Matutano, A. Wood, M. Johnson, X. Vidal Asensio, B. Baragiola, A. Reinhard, A. Lemaitre, J. Bloch, A. Amo, B. Besga, M. Richard, and T. Volz, *ArXiv e-prints* (2017), arXiv:1712.05551 [cond-mat.mes-hall].
- ²⁷ M. Khazali, K. Heshami, and C. Simon, *Journal of Physics B: Atomic, Molecular and Optical Physics* **50**, 215301 (2017).